ADVANCED FUNCTIONAL MATERIALS
www.afm-journal.de

Gold Nanocage-Based Dual Responsive "Caged Metal Chelator" Release System: Noninvasive Remote Control with Near Infrared for Potential Treatment of Alzheimer's Disease

*Peng Shi, Meng Li, Jinsong Ren, and Xiaogang Qu**

Metal ions have been demonstrated to participate in the pathology of Alzheimer's disease (AD): amyloid-β peptide (Aβ) aggregation and formation of neurotoxic reactive oxygen species (ROS), such as H_2O_2. Metal chelator can block ROS formation and inhibit metal induced Aβ aggregation. Metal-ion chelation therapy as a compelling treatment for AD has been extensively studied. However, most chelators are not suitable for AD treatment because of their poor permeability of the blood–brain barrier and their limited ability to differentiate toxic metals associated with Aβ plaques from those associated with normal metal homeostasis. Here, a novel dual-responsive "caged metal chelator" release system based on gold nanocage (AuNC) for AD treatment is reported. Since arylboronic ester is redox- and thermal-sensitive, phenylboronic acid-functionalized AuNC can serve as an efficient delivery system for H_2O_2-responsive controlled release of metal chelator. The release can be further enhanced through remote control with NIR light because of the high near-infrared absorbance of AuNC. The smart system can effectively inhibit Aβ aggregate formation, decrease cellular ROS, and protect cells from Aβ-related toxicity. In light of these advantages, this design provides new insights into noninvasive remote control with NIR to improve therapeutic efficacy for treatment of Alzheimer's disease.

1. Introduction

Alzheimer's disease (AD) is a progressive and fatal brain disease that is the most common form of dementia.[1] Although the molecular mechanisms of AD pathogenesis have not been clearly understood due to its complexity, recent advances have demonstrated that metal ions, such as $Cu^{+/2+}$, Zn^{2+}, and $Fe^{2+/3+}$, participate in two processes related to pathology: amyloid-β peptide (Aβ) aggregation[2] and formation of neurotoxic reactive oxygen species (ROS), such as hydrogen peroxide (H_2O_2).[3] Due to its ability to block ROS formation and inhibit metal induced Aβ aggregation, metal-ion chelation therapy as a compelling treatment for AD has been extensively studied.[4] However, most of the chelators are not suitable as chemical probes and potential therapeutics for AD[5] because of their poor permeability of the blood–brain barrier (BBB)[6] and their limited ability to differentiate toxic metals associated with Aβ plaques from those associated with normal metal homeostasis.[7] Therefore, their long-term clinical use is limited by an adverse side effect, subacute myelooptic neuropathy (SMON).[5] To this end, a novel design of using a "caged prochelator" as an agent that does not interact with metal ions until activated to its chelator form under certain specific conditions, such as UV photoirradiation at the site of Aβ production and specifically target metal ions in the Aβ-metal complex.[8] Moreover, bifunctional molecules with both amyloid-binding and metal-chelating moieties were also designed.[9] However, no clear-cut clinical evidence for the bifunctional effect on AD has been demonstrated and it is demanding to develop more efficient and safe drug release system against AD.

Drug delivery with controllable release using nanoscale carriers has received much attention in recent years.[10] Nanoparticles based delivery system shows advantages on reduced drug toxicity, site-specific delivery, improved biodistribution, and therapeutic efficacy. Recent progress in brain-targeted drug delivery using nanoparticles holds promise in improving drug efficacy and reduce drug side effect.[11] Previous studies have indicated that nanoparticles have the potential to cross the BBB.[12] These insights into nanoparticle transport have lent a strong impetus to chelation therapy in AD by overcoming the limitation mentioned above.[13] We and others have introduced novel concept of using controlled-release systems to realize target delivery of AD therapeutic agents.[8] In a previous report, we demonstrated a H_2O_2-responsive controlled-release system using mesoporous silica nanoparticle for AD therapy, holding promise in combating these diseases.[14]

P. Shi, M. Li, Prof. J. Ren, Prof. X. Qu
Laboratory of Chemical Biology
Division of Biological Inorganic Chemistry
State Key Laboratory of Rare Earth Resource Utilization
Changchun Institute of Applied Chemistry
Graduate School of the Chinese Academy of Sciences
Chinese Academy of Sciences
Changchun, Jilin 130022, China
E-mail: xqu@ciac.jl.cn

DOI: 10.1002/adfm.201301015

As a novel nanocontainer, gold nanocage (AuNC) with hollow interiors, porous walls, and tunable localized surface plasmon resonance (LSPR) peaks in the near-infrared (NIR) region, represent a new promising platform for therapeutic applications.[15] Au surfaces can be readily functionalized with a variety of molecules and ligands using the well-established thiolate-Au chemistry.[16] Therefore, stimuli-responsive "pore blockers" can be introduced to make AuNC a controllable release system. Besides, one enticing feature of AuNC-based delivery system lies in the novel property of AuNC which can effectively absorb and convert NIR light into heat. Upon NIR irradiation, the photothermal effect of AuNC leads to a rapid rise in the local temperature, resulting in the uncapping of the thermal-sensitive gatekeeper, allowing the release of the cargo molecules. Because NIR light can be readily tuned and focused, it can be spatially and temporally controlled to provide "on-command" drug delivery.[17] Up to now, a few reports have investigated AuNC based system for cancer therapy.[18] Despite these achievements, the utility of AuNC-based devices for other diseases therapy is still in its infancy.

Considering that arylboronic ester is redox-[19] and thermal-sensitive,[20] here we report a biocompatible platform based on AuNC to realize target delivery of AD therapeutic agents triggered by two different inputs. One advantage of this novel strategy is that metal chelator can be released by the elevated production of H_2O_2 caused by deviant Aβ-metal interactions; thus, it could be beneficial for managing a metal burden at locations of disease progression without interfering with the healthy metal homeostasis and stimulating widespread metal redistribution.[8c,g] More importantly, the new AuNC-based design can further enhance chelator release through noninvasive remote control with NIR light.[21] It should be noted that our concept based on AuNC with hollow interiors and porous walls is a general method to deliver not only small chelator molecule but also therapeutic β-sheet breaker peptide for AD treatment. In addition, utilizing the strong NIR optical absorption ability of AuNC to generate local heat may also act as an effective mean to dissolve amyloid deposits of Aβ.[22] To the best of our knowledge, no attempt has been made using the photothermal property of AuNC to realize the dual-responsive enhanced drug release for AD therapy.

2. Results and Discussion

We have successfully prepared human IgG capped AuNC (AuNC–IgG) according to our previously reported procedure with a minor modification.[14] As illustrated in **Figure 1**, we prepared amino-functionalized AuNC (AuNC–NH_2) by covalently grafting 2-aminoethanethiol onto the surface of AuNC. Subsequently, 4-carboyphenylboronic acid was condensed with AuNC–NH_2 to afford phenylboronic acid functionalized AuNC (AuNC–PBA). We also chose human IgG (≈150 kD), the hydrodynamic diameter of which was about 11 nm,[23] as the nanoscopic cap. This kind of glycoprotein could be linked to AuNC–PBA through the formation of boronate ester bond[14,24] between vicinal diols and phenylboronic acid.[25] Importantly, the opening protocol and delivery of the entrapped guest depends on two inputs. We have elucidated one opening

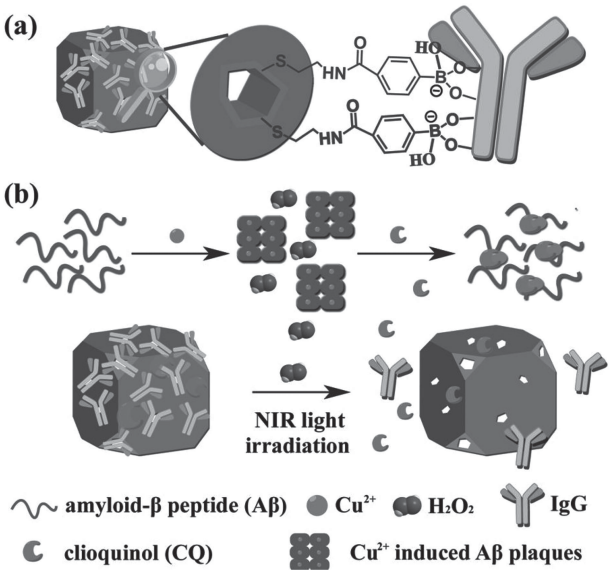

Figure 1. a) Illustration of IgG capped AuNC (AuNC–IgG). b) Schematic representation of H_2O_2-fueled and photothermal-responsive release of guest molecules clioquinol (CQ) from AuNC–IgG. CQ can chelate Cu^{2+} to disassemble amyloid-β peptide (Aβ) plaques and inhibit H_2O_2 production.

protocol in our previous report that H_2O_2 could oxidize arylboronic esters to phenols, resulting in the release of IgG and the guest molecules after that.[14,19] At the same time, plasmonic heating could also cause cleavage of the boronic ester linkage.[20] Owing to the strong photothermal effect of AuNC, NIR light irradiation can be used as another suitable opening protocol to realize remote control release. Therefore, it is expected that the release of entrapped guest would be sensitive to the concentration of H_2O_2 and photothermal effect as well.

The drug container, AuNC–PBA, was firstly prepared with careful characterization. For all of the experiments, we used AuNC–PBA about 50 nm in edge length as shown in **Figure 2**a,d. Scanning transmission electron microscopy determined that the pore size was about 5–8 nm (Figure S1, Supporting Information). By changing Au/Ag alloy aspect ratio, the LSPR peak of the obtained AuNC was tuned to about 795 nm to match the central wavelength of the NIR irradiation source (Figure S2, Supporting Information). The surface functionalization of AuNC was monitored by Fourier transform infrared (FTIR) spectrophotometer analyses (Figure S3, Supporting Information). The strong –CO–NH– (1635 cm^{-1}, 1537 cm^{-1}) vibrations in the FTIR spectrum indicated that phenylboronic acid was covalently grafted onto the AuNC surface successfully. The energy-dispersive X-ray spectroscopy (EDS) analysis also supported the presence of S and B in the as-prepared nanoparticles (Figure S4, Supporting Information). The capping of the porous walls of AuNC–PBA by IgG was characterized with transmission electron microscopy (TEM) measurements. As shown in Figure 2b,c, a relatively uniform coating on the surface of AuNC indicated that IgG was linked to AuNC–PBA successfully through the formation of boronate ester bond. Dynamic light scattering (DLS) indicated that the AuNC–IgG was well distributed. Furthermore, compared to the bare AuNC,

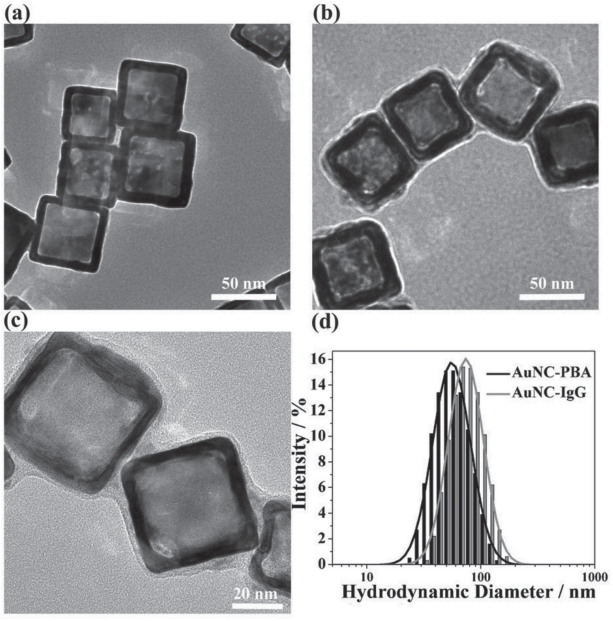

Figure 2. TEM image of as-synthesized a) AuNC and b,c) AuNC–IgG. d) DLS profile of AuNC–PBA and AuNC–IgG in PBS (10 mM, pH 7.4).

IgG attachment made a slight shift in the characteristic absorbance spectrum of the nanoparticle (Figure S5, Supporting Information) with an increased hydrodynamic radius (Figure 2d).[26] Additionally, to obtain more insight into the nanoparticles, the surface charge was examined using ζ potential measurement in distilled H_2O. As predicted in Figure S6, Supporting Information, AuNC–IgG showed a negative charge over the surface. The negative charge and smaller size provided the nanoparticle with the potential ability to cross the BBB.[27] Quantification of the density of IgG anchored on AuNC was accomplished by thermogravimetric analysis (TGA) (Figure S7, Supporting Information), which corresponded to about 88.5 mg g^{-1} AuNC.

It is known that H_2O_2 is a powerful oxidizing agent and can serve as an effective etchant for metal. To ensure the stability and reliability of our system both in vitro and in vivo, we firstly investigated the influence of H_2O_2 on samples of AuNC with the LSPR peaks at 795 nm. After incubating the sample with 1 mM H_2O_2 for 24 h on a shaker, a UV-vis spectrum was measured for the reaction. As shown in **Figure 3**a, neither the position nor intensity of the LSPR peak were effected, indicating that H_2O_2 did not dissolve Ag from 795 nm AuNC. TEM images also demonstrated that there was no obvious change in the structure of AuNC (Figure 3b). This is because a large portion of Ag in the Au–Ag alloy walls is less reactive. It is difficult for H_2O_2 to dissolve Ag from Au–Ag alloy walls of AuNCs, especially for the 795 nm AuNCs in which the percentages of Ag is low. The results were consistent with a previous report[28] and validated that AuNC with the LSPR peaks at 795 nm is stable in 1 mM H_2O_2 solution.

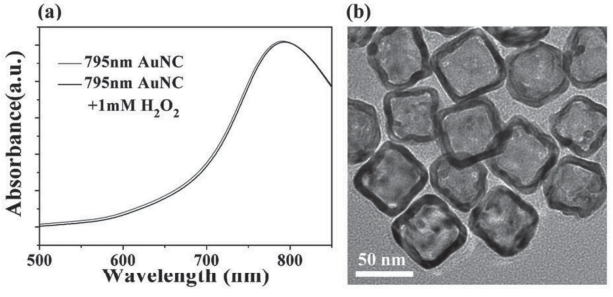

Figure 3. a) UV-vis absorption spectra of 795 nm AuNC before and after incubating with 1 mM H_2O_2 for 24 h. b) TEM image of 795 nm AuNC after incubating with 1 mM H_2O_2 for 24 h.

To investigate the stimuli-responsive drug release from the AuNC–IgG, fluorescein (FL) was used as the guest molecule to be encapsulated inside AuNC–IgG. Dye loading was accomplished by soaking AuNC–PBA in a solution of FL to allow the guest molecules to diffuse into the AuNC. The closure reaction was performed by the addition of IgG to block the pores. The excess dyes were removed by centrifugation and repeated washing with phosphate buffered saline (PBS, 10 mM, pH 7.4). Recent studies have demonstrated that cells may have phagosomes which are much more oxidizing than they are acidic, and have H_2O_2 concentrations of up to 1 mM.[19] Our release experiments were performed in PBS (10 mM, pH 7.4) with different concentrations of H_2O_2. For many practical drug delivery systems, "zero-premature release" and "stimuli-responsive controlled release" of the pharmaceutical cargo are two very important prerequisites that impact the therapeutic efficacy and cytotoxicity of drug delivery.[29] As shown in **Figure 4**a, the absorbance of FL was essentially constant in the absence of external stimuli at room temperature, indicating that IgG acted as an efficient cap for retention of guest molecules with negligible leakage. Release of the encapsulated dyes depends on the degradation of arylboronic ester and the addition of H_2O_2 could activate the capped system. Figure 4a showed that the amount of the dye released reached about 60% after 12 h for incubation upon 1 mM H_2O_2, whereas about 32% release were obtained in the same amount of time with 0.5 mM H_2O_2. To further confirm that the release was H_2O_2-concentration dependent, we tested the release experiment in a higher concentration (5 mM H_2O_2). The amount of the dye released reached about 74% in the same amount of time. Besides, one key feature of our delivery system lies in the AuNC, which can effectively absorb and convert NIR light into heat, cleaving the boronic ester linkage and enhancing the drug release. Indeed, a promotional effect of NIR irradiation on the dye release was observed experimentally. IgG capped FL loaded AuNC were incubated in PBS (10 mM, pH 7.4) with 0.5 mM H_2O_2 for 2 h and then irradiated for 5 min at 0.6 W cm^{-2} with an 808 nm NIR laser. A burst release of FL up to 54% was observed within 1 h. In comparison, only 20% FL was released without irradiation (Figure 4b). These results showed that NIR light did enhance the drug release. We also obtained the same results (Figure S8, Supporting Information) when monitoring the release process of the metal chelator, clioquinol (CQ), from AuNC–CQ–IgG in 2% (v/v) methanol/PBS solution.

To verify the feasibility of the AuNC–IgG system for AD therapeutic applications, we chose CQ as guest molecule to study its effect on Aβ aggregation and H_2O_2 formation. CQ, as a metal chelating compound, has been widely studied and achieved success in transgenic mice and in clinical trials.[4]

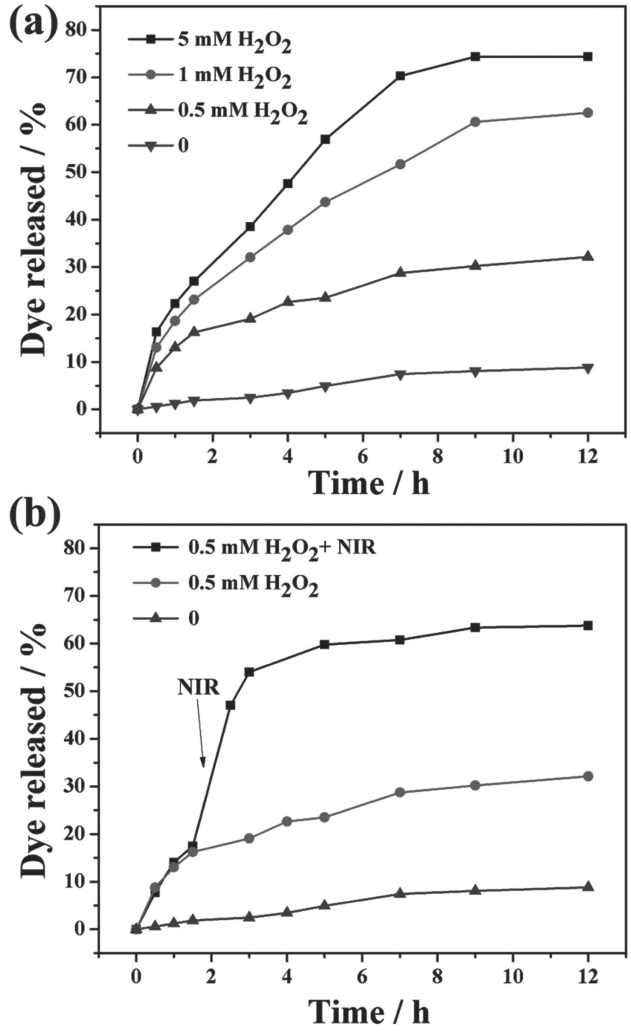

Figure 4. Release profiles of fluorescein from AuNC–IgG, a) triggered by different concentrations of H_2O_2 and b) triggered by 0.5 mM H_2O_2 with or without 5-min NIR irradiation (0.6 W cm^{-2}, 808 nm).

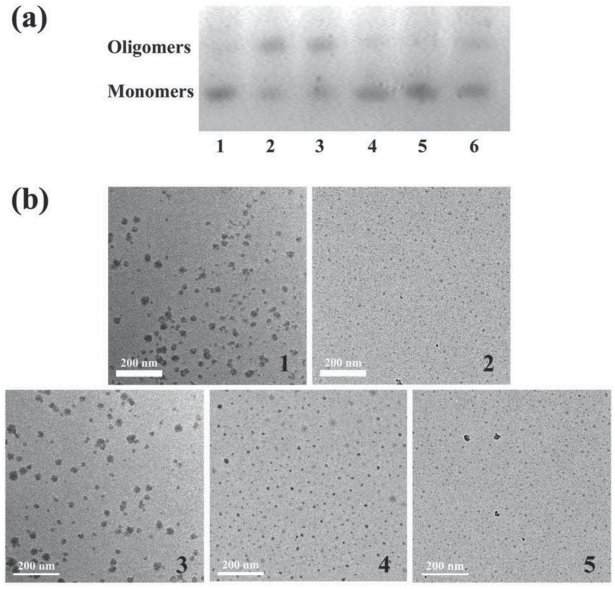

Figure 5. Determination of the inhibition effects of AuNC–CQ–IgG on the Cu^{2+}-induced Aβ aggregation a) by native-PAGE: 1) control (Aβ), 2) Aβ+Cu^{2+}, 3) Aβ+Cu^{2+}+AuNC–CQ–IgG, 4) Aβ+Cu^{2+}+AuNC-CQ-IgG+H_2O_2, 5) Aβ+Cu^{2+}+AuNC–CQ–IgG+H_2O_2 under 5-min NIR irradiation (0.6 W cm^{-2}, 808 nm), 6) Aβ+Cu^{2+}+CQ; b) by TEM images: 1) Aβ+Cu^{2+}, 2) Aβ+Cu^{2+}+CQ, 3) Aβ+Cu^{2+}+AuNC–CQ–IgG, 4) Aβ+Cu^{2+}+AuNC–CQ–IgG+H_2O_2 5) Aβ+Cu^{2+}+AuNC–CQ–IgG+H_2O_2 under 5-min NIR irradiation (0.6 W cm^{-2}, 808 nm). [Aβ] = 10 μM, [Cu^{2+}] = 10 μM, [CQ] = 20 μM, [AuNC–CQ–IgG] = 1 mg mL^{-1}, [H_2O_2] = 1 mM. Buffer: 10 mM HEPES, 150 mM NaCl, pH 6.6.

Firstly, we studied the inhibition effect of the AuNC–CQ–IgG on the Cu^{2+}-induced Aβ aggregation with native polyacrylamide gel electrophoresis (PAGE) assay.[30] Aβ-metal complex or Aβ-metal complex treated with CQ was incubated at 37 °C for 24 h before measurements. As shown in the native gel (**Figure 5**a), after incubation of Aβ with Cu^{2+} for 24 h, the monomer band became weaker while the oligomer band became stronger (lane 2), suggesting that Aβ1–40 had aggregated into higher ordered oligomers. Aβ aggregation was inhibited by CQ as demonstrated by the stronger monomer band in the native gel (lane 6). On the other hand, the presence of AuNC–CQ–IgG itself did not suppress metal-induced Aβ aggregation (lane 3). However, in the presence of H_2O_2, the monomer band became stronger due to the release of CQ (lane 4). Importantly, these strong chelators with poor targeting likely interacts with beneficial biometal and affects the normal physiological functions of essential metal-requiring metalloenzymes, thereby promoting undesirable side effects.[5,7] However, using the excessive ROS, which produced by metal-Aβ species, can be an effective way to realize the targeted treatment of AD without removing vital metals from other biological systems. Furthermore, the stronger monomer band in lane 5 compared with lane 4 indicated that AuNC–CQ–IgG showed higher inhibition efficacy under NIR light irradiation. These results were consistent with the release experiments that NIR light could enhance the drug release to realize higher therapeutic efficacy. Compared with the mesoporous silica nanoparticle based drug delivery system we previously reported,[14] the new design based on AuNC could realize spatial/temporal controlled release. To confirm the results obtained by electrophoresis assay, metal-induced Aβ aggregates were studied by TEM (Figure 5b) to give detailed morphological changes. In the Aβ sample with Cu^{2+}, a great amount of amorphous aggregates was detected after 24 h incubation. Again, AuNC–CQ–IgG itself showed little effect on the Aβ–Cu^{2+} aggregation, while in the presence of H_2O_2 and NIR light, AuNC–CQ–IgG strongly inhibited Aβ aggregation as illustrated by the fewer amorphous aggregates. All above results validated that our dual-responsive design can effectively inhibit the Cu^{2+}-induced Aβ aggregation. The same results were also observed by atomic force microscope (Figure S9, Supporting Information).

The formation of ROS by Aβ–Cu^{2+} has been suggested as another proposed mechanism of AD pathogenesis.[3] ROS can cause oxidative stress that would trigger a series of damages of cellular components such as DNA, lipids, and proteins.[31] We investigated the effect of AuNC–CQ–IgG against ROS.

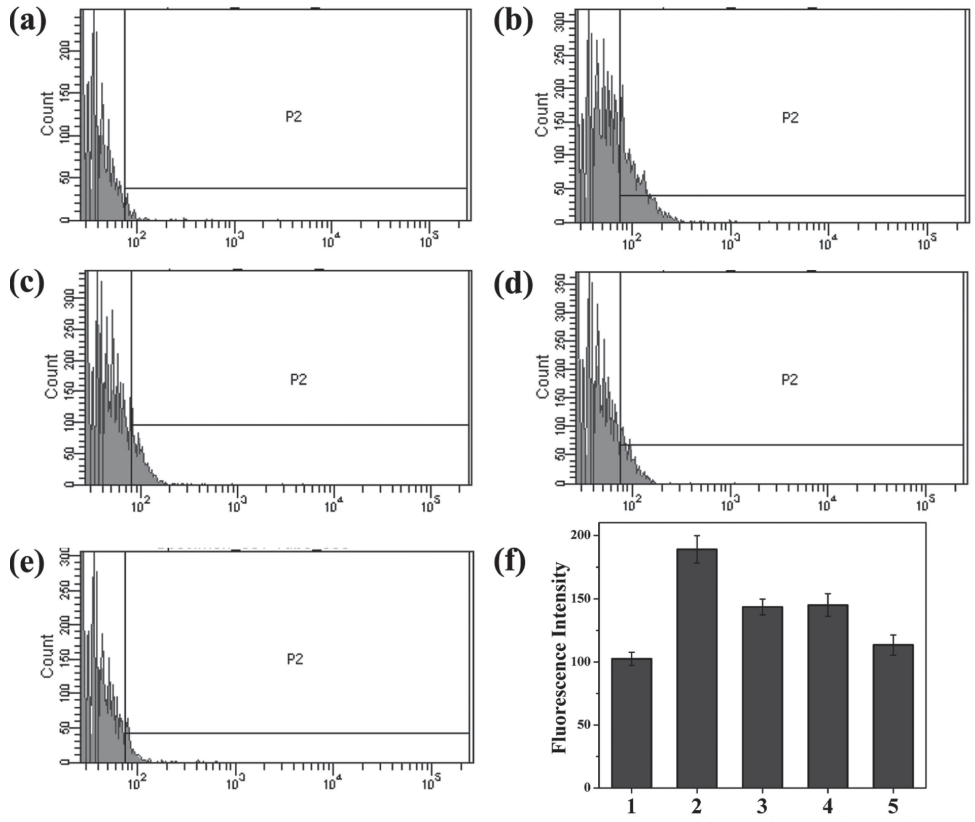

Figure 6. Cells were treated with 5 μM Aβ+Cu^{2+} in the absence or presence of AuNC–CQ–IgG for 48 h and ROS generation was measured using DCF fluorescence. Flow cytometry analysis to monitor the changes of intracellular ROS: a) control, b) Aβ+Cu^{2+}, c) Aβ+Cu^{2+} with CQ, d) Aβ+Cu^{2+} in the presence of AuNC–CQ–IgG without NIR irradiation, e) Aβ+Cu^{2+} in the presence of AuNC–CQ–IgG with 3-min NIR irradiation (0.6 W cm^{-2}, 808 nm). f) Quantification of the changes of intracellular ROS: 1) control, 2) Aβ+Cu^{2+}, 3) Aβ+Cu^{2+} with CQ, 4) Aβ+Cu^{2+} in the presence of AuNC–CQ–IgG without NIR irradiation, 5) Aβ+Cu^{2+} in the presence of AuNC–CQ–IgG with 3-min NIR irradiation (0.6 W cm^{-2}, 808 nm). Control: Aβ+Cu^{2+}-untreated cells, [Aβ] = 5 μM, [Cu^{2+}] = 5 μM, [CQ] = 10 μM, [AuNC–CQ–IgG] = 0.5 mg mL^{-1}.

Firstly, a suitable NIR power at which the living cells would not be damaged but the release of drug could be efficiently triggered is a prerequisite for our system used in vivo. As a result, power density of 0.6 W cm^{-2} was used throughout the experiments due to the not obvious cytotoxicity (Figure S10, Supporting Information). DCFH-DA (dichlorofluorescin-diacetate) was used as a probe for intracellular ROS because it diffuses into cells and becomes fluorescent DCF (dichlorofluorescin) via oxidation by intracellular ROS. As shown in **Figure 6**a–e, the changes of intracellular ROS were monitored by flow cytometry. Quantification was further given in Figure 6f. Exposure of the cells to 5 μM Aβ–Cu^{2+} complex increased the content of ROS to 183% relative to Aβ–Cu^{2+} untreated control cells. Treatment of the cells with CQ (10 μM) or AuNC–CQ–IgG (0.5 mg mL^{-1}) caused levels of ROS to diminish by 42% and 40%, respectively, compared to cells exposed only to Aβ–Cu^{2+}. Moreover, when treating the cells with AuNC–CQ–IgG under NIR light irradiation, there was an enhanced decrease in the level of ROS. The level of ROS did not vary among cells treated solely with AuNC–IgG (0.5 mg mL^{-1}), Aβ (5 μM), or Cu^{2+} (5 μM) (Figure S11, Supporting Information). Based on these results, our system can be effective free-radical scavenger.

The success in inhibiting Aβ aggregate formation and decreasing intracellular ROS prompted us to examine whether our delivery system could work in living cells. We further studied the effects of this delivery system on Aβ-induced cytotoxicity using rat pheochromocytoma PC12 cells by the methylthiazolyl tetrazolium (MTT) method.[32a] All assays were conducted under the same conditions and data were normalized using the results from cells not treated with Aβ–Cu^{2+}, which acted as a positive control. Treatment of the cells with 5 μM Aβ–Cu^{2+} reduced the cell viability to 41% (**Figure 7**). In the presence of 10 μM CQ, the survival of the cells increased to about 70%. To simulate the process of drug delivery in vivo, the materials were added to cells after stirring in 2% (v/v) methanol/PBS solution for 6 h. Under this condition, non-gated CQ-loaded AuNC showed little protection effect on cell viability due to the release during drug delivery. Meanwhile, AuNC–CQ–IgG could increase the survival of the cells to about 66%, indicating that our stimuli-responsive controlled-release systems showed "zero premature release" property could potentially reduce the non-target biometal binding and alleviate the side-effect and enhance the drug bioavailabilty. We have also investigated the feasibility to use NIR light irradiation to improve cell viability by enhancing the CQ release from AuNC–CQ–IgG. As

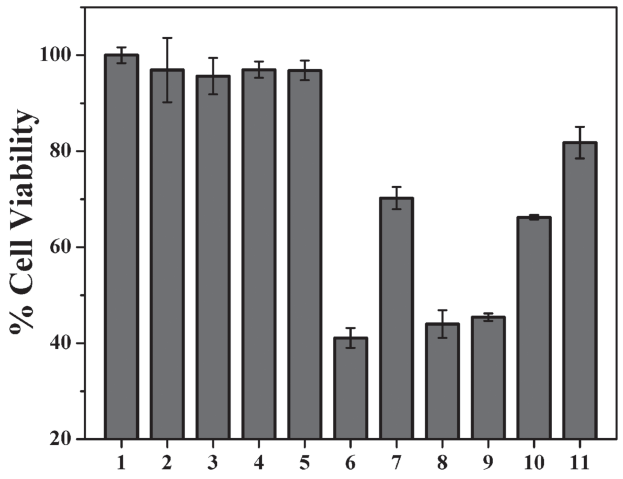

Figure 7. Protection effects of AuNC–CQ–IgG on Aβ-induced cytotoxicity of PC12 cells: 1) control, 2) Aβ, 3) Cu^{2+}, 4) AuNC–IgG, 5) AuNC–IgG with 3-min NIR irradiation (0.6 W cm^{-2}, 808 nm), 6) Aβ+Cu^{2+}, 7) Aβ+Cu^{2+}+CQ, 8) Aβ+Cu^{2+}+AuNC–IgG, 9) Aβ+Cu^{2+}+non-gated CQ-loaded AuNC, 10) Aβ+Cu^{2+}+AuNC–CQ–IgG, 11) Aβ+Cu^{2+}+AuNC–CQ–IgG with 3-min NIR irradiation (0.6 W cm^{-2}, 808 nm). Control: Aβ+Cu^{2+}-untreated cells, [Aβ] = 5 μM, [Cu^{2+}] = 5 μM, [CQ] = 10 μM, [AuNC–CQ–IgG] = 0.5 mg mL^{-1}.

expected, the viability of cells dramatically increased to 81% upon NIR light irradiation. The experiments in the presence of NIR light irradiation showed higher therapeutic efficacy when compared with the ones without NIR irradiation. In vitro studies have shown the feasibility of using this nanocarrier as a noninvasive remote controlled drug delivery system with high spatial/temporal resolution.

3. Conclusions

A novel dual-responsive "caged metal chelator" release system based on AuNC for AD treatment was presented. Since arylboronic ester is redox- and thermal-sensitive, phenylboronic acid-functionalized AuNC can serve as an efficient delivery system for H_2O_2-responsive controlled release of metal chelator. Intriguingly, owing to the high near-infrared absorbance of AuNC, the chelator release can be enhanced through remote control with NIR light. The smart system can effectively inhibit Aβ aggregate formation, decrease cellular ROS, protect cells from Aβ-related toxicity, and potentially overcome strong side effect of metal chelator after long-term use. Furthermore, as demonstrated in a previous report, the photothermal effects of AuNC can also act as an effective means to dissolve amyloid deposits of Aβ. In light of these advantages, our work may promote design of noninvasive remote control systems with NIR for Alzheimer's disease treatment.

4. Experimental Section

Materials and Instrumentation: Dimethyl sulfoxide (DMSO), ethylene glycol, and ethanol were all purchased from Beijing Chemicals (Beijing, China). $AgNO_3$ (more than 99%), PVP (powder, average Mr E 29 000 or 55 000), 2-aminoethanethiol, 4-carboyphenylboronic acid, and $HAuCl_4$–$3H_2O$ (99.9+%) were all purchased from Sigma Aldrich (Boston, MA, USA). N-hydroxysuccinimide (NHS) and 1-ethyl-3-(3-dimethylaminopropyl) carbodiimide hydrochloride (EDC) were purchased from Pierce Biotechnology. 1,1,1,3,3,3-Hexafluoro-2-propanol (HFIP) were obtained from Acros Organics. Nanopure water (18.2 MΩ cm^{-1}, Millpore Co., USA) was used in all experiments and to prepare all buffers.

FTIR analyses were carried out on a Bruker Vertex 70 FT-IR Spectrometer. TEM images were recorded using a FEI TECNAI G2 20 high-resolution transmission electron microscope operating at 100 kV. To determine the composition of the as-prepared samples, in situ EDS analysis was performed using a HITACHI S-4500 instrument. UV-vis spectroscopy was carried out with a JASCO V-550 UV/vis spectrometer. Fluorescence measurements were carried out on a JASCO FP-6500 spectrofluorometer. DLS measurements were performed on a Malvern Zetasizer NanoS apparatus equipped with a 4.0 mW laser operating at $\lambda = 633$ nm. All samples were measured at a scattering angle of 90° with particle concentration of about 0.2 mg mL^{-1} at 25 °C. TGA was recorded with a RIGAKU Standard type with a heating rate of 10 °C min^{-1} from room temperature to 800 °C. A CWdiode laser (LSR808NL-2000) with wavelength of 808 nm was used for the laser irradiation experiment.

Synthesis of Gold Nanocage: AuNC were synthesized by means of the galvanic replacement reaction between Ag nanocubes and $HAuCl_4$ according to a previously reported method.[33] Briefly, 500 μL of the Ag nanocubes (3 nM) was added to 5 mL of deionized water containing poly (vinyl pyrrolidone) (PVP, 1 mg mL^{-1}) hosted in a 50 mL flask under magnetic stirring and then heated to boil for 10 min. In the meantime, an aqueous solution of $HAuCl_4$ (0.5 mM) was prepared. The $HAuCl_4$ was added to the flask at a rate of 45 mL h^{-1} until the solution had an optical extinction peak at 795 nm as confirmed by UV spectroscopy. The solution was refluxed for another 30 min until the color of the reaction was stable. Once cooled to room temperature, the sample was centrifuged and washed with saturated NaCl solution to remove AgCl and with water several times to remove PVP and NaCl.

Synthesis of Phenylboronic Acid Functionalized Gold Nanocage: AuNC–PBA was prepared by a two-step method. The PVP was first replaced on nanocages with 2-aminoethanethiol to obtain AuNC-NH_2. The purified AuNC–NH_2 (10 mg) was dispersed in 10 mL DMSO. 8 mg 4-carboxyphenylboronic acid was reacted with 10 mg NHS and 20 mg EDC in 4 mL DMSO, stirring at room temperature for 30 min before adding to the AuNC–NH_2 suspension. The mixture was stirred at room temperature for another 24 h, followed by filtration and washing with DMSO, water, and ethanol.

Fluorescein (Clioquinol) Loading and IgG Capping: The purified AuNC–PBA was stirred vigorously (vortex stirrer) in a solution of fluorescein (0.5 mM) in PBS (10 mM, pH 7.4) for 24 h (clioquinol loading was performed in ethanol). Drug filled AuNC–PBA was harvested by centrifugation and resuspended in PBS. Then, IgG were added to the suspension, and the mixture was stirred for another 12 h, followed by centrifuging (9000 rpm) and repeated washing with PBS solution (10 mM, pH 7.4). All the washing solutions were collected, and the loading of fluorescein (clioquinol) was calculated from the difference in the concentration of the initial and left fluorescein (clioquinol). The loading capability is 57 μg FL mg^{-1} AuNC and 11 μg CQ mg^{-1} AuNC.

Fluorescein (Clioquinol) Release Experiments: AuNC–FL–IgG (AuNC–CQ–IgG) were dispersed in PBS (10 mM, pH 7.4) with or without stimulus. At predetermined time intervals, aliquots were taken from the suspension and centrifuged, the supernatants were measured by UV-vis spectrum. The delivery of dye from the pore to the buffer solution was monitored via the absorbance band of the dye centered at 553 nm (325 nm for CQ). The release process of CQ from AuNC–CQ–IgG was performed in 2% (v/v) methanol/PBS solution.

Aβ Preparation: Lyophilized synthetic human Aβ1–40 (lot no. U10012) was purchased from American Peptide. The preparation of Aβ was according to the previous reports.[32] First, the powered Aβ peptide was dissolved in 1,1,1,3,3,3-hexafluoro-2-propanol (HFIP) at the concentration of 1 mg mL^{-1}. Then, the solution was shaking at

4 °C for 2 h in a sealed vial. The obtained sample was then stored at −20 °C as a stock solution. Before use, the solvent HFIP was removed by evaporation under a gentle stream of nitrogen and the peptide was dissolved in distilled, deionized water. Cu^{2+} induced aggregation of Aβ 1–40 was accomplished by mixing an aliquot of the peptides and $CuCl_2$ at a molar ratio of 1:1 into 10 mM HEPES (150 mM NaCl, pH 6.6) at 37 °C for 24 h.

Native Polyacrylamide Gel Electrophoresis: Aβ40 peptide (10 μM) under different conditions was incubated at 37 °C for 24 h. Native PAGE was carried out using a 12% gel. Gels were run in a Tris/Glycine system and followed by silver staining.

Transmission Electron Microscopy: Samples were spotted onto carbon-coated copper grids for 30 min. The grids were blotted with filter paper to remove excess buffer and the sample was stained with 1.5% (w/v) phosphotungstic acid (pH 7.4). Grids were blotted again and air-dried before analysis on a transmission electron microscope, operating with a voltage of 100 kV.

Intracellular Determination of ROS: The generation of reactive oxygen radicals was monitored using 2′,7′-dichlorofluorescein diacetate (DCFH-DA). This dye is a nonfluorescent compound which reacts with intracellular free radicals. The product, dichloro-fluorescein (DCF), is a fluorophor. The DCF fluorescence intensity correlates with the amount of intracellular reactive oxygen radicals. To perform the test, DCFH-DA solution (20 mM) was added to the cells, and the mixture was incubated at 37 °C for 1 h. The cells were then washed twice with PBS and finally, the fluorescence intensity was monitored by flow cytometric analysis and fluorescence spectrofluorometer.

Cell Toxicity Assays: PC12 cells (rat pheochromocytoma, American Type Culture Collection) were cultured in IMDM (Gibco BRL) medium supplemented with 5% FBS, 10% horse serum in a 5% CO_2 humidified environment at 37 °C. For the MTT (3-(4,5-dimethylthiazol-2-yl)-2,5-diphenyltetrazolium bromide, Sigma-Aldrich) assay, cells were plated at a density of 10 000 cells per well on 96-well plates for 24 h, followed by introduction of Aβ (5 μM), $CuCl_2$ (5 μM), and CQ or AuNC–CQ–IgG with or without 0.6 W cm^{-2}, 808 nm NIR laser irradiation for 3 min. After 48 h, the cells were treated with 10 μL MTT (5 mg mL^{-1} in PBS) for 4 h at 37 °C and then were lysed in DMSO for 10 min at room temperature in the dark. Absorbance values of formazan were determined at 570 nm with an automatic plate reader.

Supporting Information

Supporting Information is available from the Wiley Online Library or from the author.

Acknowledgements

Financial support was provided by 973 Project (2011CB936004, 2012CB720602) and NSFC (221210002, 91213302).

Received: March 22, 2013
Published online: June 10, 2013

[1] K. Blennow, M. J. de Leon, H. Zetterberg, *Lancet* **2006**, *368*, 387.
[2] a) M. A. Lovell, J. D. Robertson, W. J. Teesdale, J. L. Campbell, W. R. Markesbery, *J. Neurol. Sci.* **1998**, *158*, 47; b) A. I. Bush, *Trends Neurosci.* **2003**, *26*, 207; c) C. S. Atwood, R. D. Moir, X. D. Huang, R. C. Scarpa, N. M. E. Bacarra, D. M. Romano, M. K. Hartshorn, R. E. Tanzi, A. I. Bush, *J. Bio. Chem.* **1998**, *273*, 12817; d) A. I. Bush, W. H. Pettingell, G. Multhaup, M. D. Paradis, J. P. Vonsattel, J. F. Gusella, K. Beyreuther, C. L. Masters, R. E. Tanzi, *Science* **1994**, *265*, 1464.
[3] a) J. Dong, C. S. Atwood, V. E. Anderson, S. L. Siedlak, M. A. Smith, G. Perry, P. R. Carey, *Biochemistry* **2003**, *42*, 2768; b) L. Guilloreau, S. Combalbert, A. Sournia-Saquet, H. Mazarguil, P. Faller, *ChemBioChem* **2007**, *8*, 1317; c) X. D. Huang, C. S. Atwood, M. A. Hartshorn, G. Multhaup, L. E. Goldstein, R. C. Scarpa, M. P. Cuajungco, D. N. Gray, J. Lim, R. D. Moir, R. E. Tanzi, A. I. Bush, *Biochemistry* **1999**, *38*, 7609; d) T. Lynch, R. A. Cherny, A. I. Bush, *Exp. Gerontol.* **2000**, *35*, 445.
[4] a) R. A. Cherny, J. T. Legg, C. A. McLean, D. P. Fairlie, X. Huang, C. S. Atwood, K. Beyreuther, R. E. Tanzi, C. L. Masters, A. I. Bush, *J. Biol. Chem.* **1999**, *274*, 23223; b) R. A. Cherny, C. S. Atwood, M. E. Xilinas, D. N. Gray, W. D. Jones, C. A. McLean, K. J. Barnham, I. Volitakis, F. W. Fraser, Y. Kim, X. Huang, L. E. Goldstein, R. D. Moir, J. T. Lim, K. Beyreuther, H. Zheng, R. E. Tanzi, C. L. Masters, A. I. Bush, *Neuron* **2001**, *30*, 665; c) S. Schäfer, F.-G. Pajonk, G. Multhaup, T. Bayer, *J. Mol. Med.* **2007**, *85*, 405.
[5] L. Cahoon, *Nat. Med.* **2009**, *15*, 356.
[6] W. M. Pardridge, *Alzheimers Dement.* **2009**, *5*, 427.
[7] A. Dedeoglu, K. Cormier, S. Payton, K. A. Tseitlin, J. N. Kremsky, L. Lai, X. Li, R. D. Moir, R. E. Tanzi, A. I. Bush, N. W. Kowall, J. T. Rogers, X. Huang, *Exp. Gerontol.* **2004**, *39*, 1641.
[8] a) H. Schugar, D. E. Green, M. L. Bowen, L. E. Scott, T. Storr, K. Bohmerle, F. Thomas, D. D. Allen, P. R. Lockman, M. Merkel, K. H. Thompson, C. Orvig, *Angew. Chem. Int. Ed.* **2007**, *46*, 1716; b) D. S. Folk, K. J. Franz, *J. Am. Chem. Soc.* **2010**, *132*, 4994; c) M. G. Dickens, K. J. Franz, *ChemBioChem* **2010**, *11*, 59; d) H. Zheng, M. B. Youdim, M. Fridkin, *J. Med. Chem.* **2009**, *52*, 4095; e) H. Zheng, M. B. Youdim, M. Fridkin, *ACS Chem. Biol.* **2010**, *5*, 603; f) M. Li, Z. Liu, J. Ren, X. Qu, *Chem. Sci.* **2012**, *3*, 868; g) L. K. Charkoudian, D. M. Pham, K. J. Franz, *J. Am. Chem. Soc.* **2006**, *128*, 12424.
[9] a) S. S. Hindo, A. M. Mancino, J. J. Braymer, Y. Liu, S. Vivekanandan, A. Ramamoorthy, M. H. Lim, *J. Am. Chem. Soc.* **2009**, *131*, 16663; b) C. Rodriguez-Rodriguez, N. Sanchez de Groot, A. Rimola, A. Alvarez-Larena, V. Lloveras, J. Vidal-Gancedo, S. Ventura, J. Vendrell, M. Sodupe, P. Gonzalez-Duarte, *J. Am. Chem. Soc.* **2009**, *131*, 1436; c) J. S. Choi, J. J. Braymer, R. P. Nanga, A. Ramamoorthy, M. H. Lim, *Proc. Natl. Acad. Sci. USA* **2010**, *107*, 21990; d) J. Geng, M. Li, L. Wu, J. Ren, X. Qu, *J. Med. Chem.* **2012**, *55*, 9146.
[10] O. C. Farokhzad, R. Langer, *ACS Nano* **2009**, *3*, 16.
[11] P. R. Lockman, R. J. Mumper, M. A. Khan, D. D. Allen, *Drug. Dev. Ind. Pharm.* **2002**, *28*, 1.
[12] S. I. Yoo, M. Yang, J. R. Brender, V. Subramanian, K. Sun, N. E. Joo, S.-H. Jeong, A. Ramamoorthy, N. A. Kotov, *Angew. Chem. Int. Ed.* **2011**, *50*, 5110.
[13] a) G. Liu, P. Men, P. L. Harris, R. K. Rolston, G. Perry, M. A. Smith, *Neurosci. Lett.* **2006**, *406*, 189; b) G. Liu, M. R. Garrett, P. Men, X. Zhu, G. Perry, M. A. Smith, *Biochim. Biophys. Acta* **2005**, *1741*, 246.
[14] J. Geng, M. Li, L. Wu, C. Chen, X. Qu, *Adv. Healthc. Mater.* **2012**, *1*, 332.
[15] Y. Xia, W. Li, C. M. Cobley, J. Chen, X. Xia, Q. Zhang, M. Yang, E. C. Cho, P. K. Brown, *Acc. Chem. Res.* **2011**, *44*, 914.
[16] Y. Xia, J. A. Rogers, K. E. Paul, G. M. Whitesides, *Chem. Rev.* **1999**, *99*, 1823.
[17] a) M. S. Yavuz, Y. Cheng, J. Chen, C. M. Cobley, Q. Zhang, M. Rycenga, J. Xie, C. Kim, K. H. Song, A. G. Schwartz, L. V. Wang, Y. Xia, *Nat. Mater.* **2009**, *8*, 935; b) G. D. Moon, S.-W. Choi, X. Cai, W. Li, E. C. Cho, U. Jeong, L. V. Wang, Y. Xia, *J. Am. Chem. Soc.* **2011**, *133*, 4762.
[18] a) L. Au, D. Zheng, F. Zhou, Z.-Y. Li, X. Li, Y. Xia, *ACS Nano* **2008**, *2*, 1645; b) J. Chen, D. Wang, J. Xi, L. Au, A. Siekkinen, A. Warsen, Z.-Y. Li, H. Zhang, Y. Xia, X. Li, *Nano Lett.* **2007**, *7*, 1318; c) B. Khlebtsov, E. Panfilova, V. Khanadeev, O. Bibikova, G. Terentyuk, A. Ivanov, V. Rumyantseva, I. Shilov, A. Ryabova,

V. Loshchenov, N. G. Khlebtsov, *ACS Nano* **2011**, *5*, 7077; d) L. Gao, J. Fei, J. Zhao, H. Li, Y. Cui, J. Li, *ACS Nano* **2012**, *6*, 8030; e) S. A. Khan, R. Kanchanapally, Z. Fan, L. Beqa, A. K. Singh, D. Senapati, P. C. Ray, *Chem. Commun.* **2012**, *48*, 6711.

[19] K. E. Broaders, S. Grandhe, J. M. Frechet, *J. Am. Chem. Soc.* **2011**, *133*, 756.

[20] E. Aznar, M. D. Marcos, R. N. Martínez-Máñez, F. l. Sancenón, J. Soto, P. Amorós, C. Guillem, *J. Am. Chem. Soc.* **2009**, *131*, 6833.

[21] P. Shi, K. Qu, M. Li, J. Wang, J. Ren, X. Qu, *Chem. Commun.* **2012**, *48*, 7640.

[22] M. Li, X. Yang, J. Ren, K. Qu, X. Qu, *Adv. Mater.* **2012**, *24*, 1722.

[23] J. Kang, G. Erdodi, J. P. Kennedy, H. Chou, L. Lu, S. Grundfest-Broniatowski, *Macromol. Biosci.* **2010**, *10*, 369.

[24] Y. Xu, Z. Wu, L. Zhang, H. Lu, P. Yang, P. A. Webley, D. Zhao, *Anal. Chem.* **2009**, *81*, 503.

[25] G. Springsteen, B. Wang, *Tetrahedron* **2002**, *58*, 5291.

[26] I.-H. Lee, H.-K. Kwon, S. An, D. Kim, S. Kim, M. K. Yu, J.-H. Lee, T.-S. Lee, S.-H. Im, S. Jon, *Angew. Chem. Int. Ed.* **2012**, *51*, 8800.

[27] a) S. Krol, *J. Controlled Release* **2012**, *164*, 145; b) G. Sonavane, K. Tomoda, K. Makino, *Colloids Surf., B* **2008**, *66*, 274.

[28] Q. Zhang, C. M. Cobley, J. Zeng, L.-P. Wen, J. Chen, Y. Xia, *J. Phys. Chem. C* **2010**, *114*, 6396.

[29] Y. Zhao, B. G. Trewyn, I. Slowing, V. S. Y. Lin, *J. Am. Chem. Soc.* **2009**, *131*, 8398

[30] a) J. Geng, C. Zhao, J. Ren, X. Qu, *Chem. Commun.* **2010**, *46*, 7187; b) J. Geng, H. J. Yu, J. S. Ren, X. G. Qu, *Electrochem. Commun.* **2008**, *10*, 1797; c) H. Yu, J. Ren, X. Qu, *ChemBioChem* **2008**, *9*, 879; d) H. J. Yu, J. S. Ren, X. G. Qu, *Biophys. J.* **2007**, *92*, 185.

[31] S. Miranda, C. Opazo, L. F. Larrondo, F. J. Munoz, F. Ruiz, F. Leighton, N. C. Inestrosa, *Prog. Neurobiol.* **2000**, *62*, 633.

[32] a) J. Geng, M. Li, J. Ren, E. Wang, X. Qu, *Angew. Chem. Int. Ed.* **2011**, *50*, 4184; b) C. Rodríguez-Rodríguez, N. Sánchez de Groot, A. Rimola, A. N. Álvarez-Larena, V. Lloveras, J. Vidal-Gancedo, S. Ventura, J. Vendrell, M. Sodupe, P. González-Duarte, *J. Am. Chem. Soc.* **2009**, *131*, 1436.

[33] S. E. Skrabalak, L. Au, X. Li, Y. Xia, *Nat. Protoc.* **2007**, *2*, 2182.